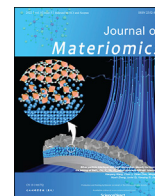




Contents lists available at ScienceDirect

Journal of Materiomics

journal homepage: [www.journals.elsevier.com/journal-of-materiomics/](http://www.journals.elsevier.com/journal-of-materiomics/)

Research paper

# Amorphous Ge-Sb-Se-Te chalcogenide films fabrication for potential environmental sensing and nonlinear photonics

Tomáš Halenkovič<sup>a, b</sup>, Marion Baillieul<sup>a, b</sup>, Jan Gutwirth<sup>a</sup>, Petr Němec<sup>a</sup>,  
Virginie Nazabal<sup>b, a, \*</sup>

<sup>a</sup> Department of Graphic Arts and Photophysics, Faculty of Chemical Technology, University of Pardubice, Studentská 573, 53210, Pardubice, Czech Republic

<sup>b</sup> Univ Rennes, CNRS, ISCR (Institut des Sciences Chimiques de Rennes) – UMR 6226, F-35000, Rennes, France



## ARTICLE INFO

## Article history:

Received 14 December 2021

Received in revised form

22 February 2022

Accepted 24 February 2022

Available online 28 March 2022

## Keywords:

Chalcogenide

Thin films

Glass

Amorphous

Optical properties

NLO

Contact angles

Sputtering

Raman

## ABSTRACT

Quaternary Ge-Sb-Se-Te chalcogenide thin films were fabricated by rf magnetron sputtering from  $\text{Ge}_{19}\text{Sb}_{17}\text{Se}_{64-x}\text{Te}_x$  ( $x = 5, 10, 15, 20$ ) sputtering targets in order to select appropriate compositions for infrared sensor and optical nonlinear applications. An influence of chemical composition and deposition parameters on the optical properties, structure and wettability was thus studied. The amorphous thin films seem to be constituted by selenide entities that can include tellurium atoms in variable proportion such as  $[\text{GeSe}_{4-x}\text{Te}_x]$  and  $[\text{SbSe}_{3-x}\text{Te}_x]$  ( $x = 0, 1, 2$ ) and Ge(Sb)-Ge(Sb) bonds according to Raman spectroscopy. Contact angle measurements of the thin films showed values of  $68\text{--}71^\circ$  for water and their surface energies in the range of  $\sim 36\text{--}39 \text{ mJ}\cdot\text{m}^{-2}$  seem suitable for surface functionalization required for photonic sensor development. Furthermore, the maximum nonlinearity at the telecom wavelength with respect to the highest figure of merit value was found for the thin film with composition  $\text{Ge}_{19}\text{Sb}_{17}\text{Se}_{56}\text{Te}_8$  having nonlinear refractive index of  $28 \times 10^{-18} \text{ m}^2\cdot\text{W}^{-1}$ . Due to their low optical bandgap energies, they may find their full interest for nonlinear optics in the mid-infrared range. Wide IR transparency in combination with high (non)linear refractive indices make these materials attractive in the field of mid-IR sensing and optical nonlinear devices.

© 2022 The Chinese Ceramic Society. Production and hosting by Elsevier B.V. This is an open access article under the CC BY-NC-ND license (<http://creativecommons.org/licenses/by-nc-nd/4.0/>).

## 1. Introduction

Amorphous chalcogenides, non-crystalline solids based on the elements of chalcogens (*i.e.* S, Se, Te), are well known for their unique properties such as low phonon energies resulting in broad transmission window, photoinduced phenomena or high optical nonlinearities without free carriers [1–3]. These make them suitable for potential applications in various fields including phase-change materials [4], artificial neural networks [5], non-linear photonics [3], optical sensors [6], mid-IR sources [7] *etc.*

Indeed, with the addition of a third element such as Sb to the Ge–Se binary system, the glassy material is stabilized by cross-links between more diverse structural entities that create

configurational changes in the system, which could promote the broadening of the glass formation domain and influence the physical properties [8]. In detail, when a small amount of Sb is added to Ge–Se system, a significant decrease in optical loss can be observed [9]. Previously, Ge-Sb-Se (herein GSS) based infrared sensor devoted to evanescent wave detection was designed and fabricated [6]. The transducer was made of two superposed amorphous thin layers. The cladding and guiding layers were of  $\text{Ge}_{31}\text{Sb}_6\text{Se}_{62}$  and  $\text{Ge}_{15}\text{Sb}_{24}\text{Se}_{61}$  for the real compositions of the sputtered thin films deposited at  $1 \times 10^{-2}$  mbar and 20 W and 10 W, respectively and presenting a refractive index contrast of  $0.33 \pm 0.02$  at  $7.7 \mu\text{m}$  [10]. Even if these two compositions have allowed the realization of efficient optical waveguides for sensor [6] and nonlinear optical applications [11],  $\text{Ge}_{12.5}\text{Sb}_{25}\text{Se}_{62.5}$  glass targets used for thin film sputtering are less resistant to thermo-mechanical stresses than  $\text{Ge}_{28.1}\text{Sb}_{6.3}\text{Se}_{65.6}$  ones. This induces a high material loss during the various stages of glass target fabrication.

Causing higher financial and temporal cost, the authors were interested in finding a pair of compositions that also meet the criteria necessary for the fabrication of a waveguide for integrated

\* Corresponding author. Univ Rennes, CNRS, ISCR (Institut des Sciences Chimiques de Rennes) – UMR 6226, F-35000, Rennes, France.

E-mail addresses: [Tomas.Halenkovic@upce.cz](mailto:Tomas.Halenkovic@upce.cz) (T. Halenkovič), [Marion.Baillieul@upce.cz](mailto:Marion.Baillieul@upce.cz) (M. Baillieul), [Jan.Gutwirth@upce.cz](mailto:Jan.Gutwirth@upce.cz) (J. Gutwirth), [Petr.Nemec@upce.cz](mailto:Petr.Nemec@upce.cz) (P. Němec), [virginie.nazabal@univ-rennes1.fr](mailto:virginie.nazabal@univ-rennes1.fr) (V. Nazabal).

Peer review under responsibility of The Chinese Ceramic Society.

optics, while being more robust from thermomechanical point of view. The (GeSe<sub>2</sub>)-(Sb<sub>2</sub>Se<sub>3</sub>) pseudo-binary system has been previously studied by Olivier et al. [12]. Subsequently, it was found that the particular composition of Ge<sub>19.4</sub>Sb<sub>16.7</sub>Se<sub>63.9</sub> for the glass target, that corresponds to (GeSe<sub>2</sub>)<sub>70</sub>(Sb<sub>2</sub>Se<sub>3</sub>)<sub>30</sub>, is suitable for natural water pollution detection sensors in mid-IR region [13] as well as for nonlinear photonics devices limiting two photon absorption at 1.55 μm from 0.37 cm · GW<sup>-1</sup> for slab waveguide and photosensitivity related to optical nonlinearity effects [12,14]. Nevertheless, the refractive index contrast of the mid-IR waveguide was lower due to mentioned composition change, with a refractive index contrast of  $\Delta n = 0.21 \pm 0.02$  at 7.7 μm between the buffer (Ge<sub>31</sub>Sb<sub>6</sub>Se<sub>63</sub>) and the guiding (Ge<sub>22</sub>Sb<sub>16</sub>Se<sub>62</sub>) layers deposited at an Ar pressure of  $5 \times 10^{-3}$  mbar and RF power of 15 W [13].

The linear and nonlinear refractive index contrast would be increased by a substitution of tellurium to selenium. Quaternary Ge-Sb-Se-Te alloys also known as GSST have already attracted the attention of some authors [15–18]. First, it is considered to be a promising replacement of Ge<sub>2</sub>Sb<sub>2</sub>Te<sub>5</sub> for high-performance phase-change material applications due to the higher 10-year data retention as reported by Wang et al. [17]. Moreover, the substitution of selenium by heavier tellurium atoms causes the decrease of lattice phonon energies broadening the transparency within mid-IR region. Thus, Te-based glasses present extended transmission in the 6–20 μm range and consequently allow the detection of the greenhouse gases absorption peaks especially at longer wavelengths than usual [19,20]. Besides that, an increasing tellurium concentration causes the rise of the linear refractive index making GSST promising materials for nonlinear optical applications [15].

In this work, the influence of chemical composition and deposition parameters on the optical properties, structure and wettability of the GSST thin films was studied and the potential application of GSST thin film for mid-IR sensing and nonlinear optical (NLO) applications is discussed.

## 2. Materials and methods

Glass-ceramics sputtering targets having compositions of Ge<sub>19</sub>Sb<sub>17</sub>Se<sub>64-x</sub>Te<sub>x</sub> ( $x = 5, 10, 15, 20$ ) were obtained by a conventional melt-quenching technique. The maximum concentration of tellurium in the GSST targets was limited by the feasibility of fabricating sputtering targets of 50 mm diameter and 3.5 mm thickness. The thermal analysis of the bulk targets was performed at 10 °C min<sup>-1</sup> by means of differential scanning calorimetry (DSC, TA Instruments DSC Q20, USA). Bulk material obtained from targets' synthesis was also used for further analysis in order to investigate potential crystallinity of sputtering targets. The X-ray diffraction (XRD) data were recorded with a X'Pert Pro Malvern Panalytical diffractometer (Cu K<sub>α</sub>, 2θ: 5°–90°, step size: 0.026°, step time: 40 s, voltage: 40 kV, current: 40 mA).

Thin films were deposited at a room temperature by rf (13.56 MHz) magnetron sputtering in Ar plasma. The substrates used for the deposition were borosilicate glass (Schott, BK7) and single crystalline silicon <100>. The former was used for spectroscopic and XRD measurements, the latter for scanning electron microscopy with energy-dispersive X-ray analyser (SEM-EDS), atomic force microscopy (AFM) and the contact angle measurements. The electrical power applied on targets was 10 and 15 W. Two different Ar pressures were maintained in the deposition chamber, specifically  $5 \times 10^{-3}$  and  $1 \times 10^{-2}$  mbar, while the Ar flow was kept constant (*i.e.* 75 sccm). In order to be able to characterize the surface of the GSST thin films by AFM or contact angle techniques, they were kept in a desiccator in the dark because whatever the composition of the layer, the impact of visible light and UV as well as the moisture on the thin layers is documented and has to be

minimized [21]. In case of both, the contact angle measurements as well as AFM, experiments are carried out with a minimum time delay after the deposition of thin films. Routinely, spectroscopic ellipsometry and AFM are performed with a highest priority compared to other experiments.

Topography of fabricated films was measured by amplitude modulated AFM (Solver Next, NT-MDT, Russia). Furthermore, chemical composition of thin films was obtained from EDS analysis using joint SEM-EDS (JEOL IT 300 LA EDS, JEOL Ltd., Japan). EDS (ZAF standardless method) remains a relatively imprecise measurement as evidenced by its expected uncertainty ( $\pm 1$  at. %) especially for thin films where the contribution of the substrate can become significant. However, in similar acquisition conditions and films of the same thickness, the composition evolution from one layer to another is generally well provided. The local structure of thin films was studied by μ-Raman scattering spectroscopy (Lab-Ram HR800, Horiba Jobin-Yvon, NJ, USA) coupled with a  $\times 100$  microscope (Olympus, Japan) with the excitation wavelength of 785 nm. Thermal population effect at low wavenumbers was minimized by means of reduction of Raman intensity according Shuker and Gammon [22].

Two variable angle spectroscopic ellipsometers (J.A. Woollam Co., Inc., Lincoln, NE, USA) were employed in order to estimate the optical bandgap energy and refractive index dispersion of the fabricated films: first working in the UV-Vis-NIR range (300–2300 nm), the other in mid-IR ( $\sim 300$ –6,000 cm<sup>-1</sup>). The fundamental absorption edge was modelled by Cody-Lorentz oscillator model (described elsewhere [23]) to fit the ellipsometry data in the UV-Vis-NIR region. Within mid-IR range, the Sellmeier model was applied setting extinction coefficient to zero. The thickness of the films on borosilicate glass (Schott, BK7) was about 800 nm ( $\pm 1\%$ ) as determined by spectroscopic ellipsometry.

Surface energy  $\sigma$  of thin films was determined following Owens-Wendt theory. Contact angles were obtained by computer controlled KSV CAM 100 USB video camera (KSV Instruments Ltd., Finland) at resolution of 640 × 480 px from curve fitting based on Young-Laplace equation of the sessile drop shape. Sessile drops of five standard liquids were recorded for 30 s immediately after the placing them onto the thin films surface. Equilibrium contact angle  $\theta_{eq}$  was considered to be established after 30 s. All the contact angle measurements were carried out at 20 °C and  $\sim 30\%$  of relative humidity. Thin films used for the contact angle measurements were deposited at the electrical power of 10 W and the Ar pressure of  $5 \times 10^{-3}$  mbar onto 2-inch silicon wafers. The thickness of these films specifically deposited for contact angle measurements was in the range of  $\sim 600$ –700 nm. Contact angle was measured on the virgin thin films stored for a short time in the light isolated desiccator in order to ensure good reproducibility of the contact angle measurements.

## 3. Results and discussion

### 3.1. Glass target characterisation

The average chemical composition of the targets is in good agreement with theoretical compositions. The DSC measurements performed with GSST glass targets have shown that the glass transition temperature  $T_g$  was decreasing with an increasing tellurium content from the initial value of 265 °C for tellurium-free composition of Ge<sub>19</sub>Sb<sub>17</sub>Se<sub>64</sub>. Obtained values of  $T_g$  for Ge<sub>19</sub>Sb<sub>17</sub>Se<sub>64-x</sub>Te<sub>x</sub> with  $x = 5, 10$  and  $15$  were 247, 232 and 222 °C respectively ( $\pm 2$  °C). The  $T_g$  variation of about 40 °C is observed for almost one quarter of selenium by tellurium substitution. These results agree with the gradual introduction of tellurium atoms in substitution for selenium atoms as the binding energies of the vitreous

network decrease compared to those formed with selenium. This substitution could also have an effect on the crosslinking of the network, but probably to a lesser extent. The change in the difference between the  $T_g$  and the crystallization onset temperature  $T_x$ , one of the possible parameters showing the thermal stability of amorphous/glassy material, is also noticeable varying from  $T_x - T_g \geq 150^\circ\text{C}$  to  $\sim 90^\circ\text{C}$  with  $x = 0$  to 15. For the last target with the highest proportion of tellurium, the distinction between its glass transition temperature and crystallization onset temperature is no longer clearly discernible, probably resulting in the formation of a glass-ceramic target. It should be noted that these large diameter bulk targets have very altered conditions of rapid cooling compared to the synthesis of glass of smaller dimensions, which exacerbates the possible formation of crystalline phases.

XRD analysis showed that obtained targets were vitreous with one exception. The diffraction peaks in the XRD patterns corresponding to  $\text{GeSe}_2$  and  $\text{Sb}_2\text{Se}_x\text{Te}_y$  (with  $x + y = 3$ ,  $x = 1$  or 2 and  $y = 1$  or 2) phases appeared for target with nominal composition of  $\text{Ge}_{19}\text{Sb}_{17}\text{Se}_{44}\text{Te}_{20}$  as shown in Fig. 1. Since the average composition of the partially crystalline target remains unchanged from the theoretical composition, the nature of the  $\text{Ge}_{19}\text{Sb}_{17}\text{Se}_{44}\text{Te}_{20}$  glass-ceramic target should marginally influence the composition of the final thin film and its deposition rate, which nevertheless needs to be verified. The very fast quenching speeds during the sputtering process of GSST films on a silicon substrate at room temperature should make it possible to obtain amorphous films even if one of the targets is partially crystallized. The insert in Fig. 1 showing the XRD

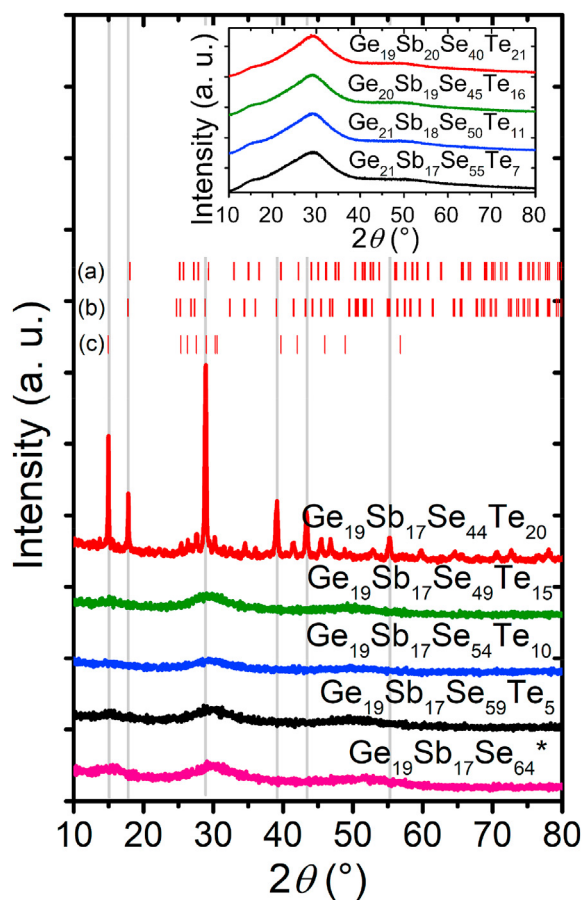


**Fig. 1.** XRD patterns of bulk GSST target materials with indicated powder diffraction patterns from crystallographic databases:  $\text{Sb}_2\text{Se}_2\text{Te}$  (a, COD ID 1008844),  $\text{Sb}_2\text{SeTe}_2$  (b, COD ID 9007591), and  $\text{GeSe}_2$  (c, ICDD 00-042-1104); Insert with XRD patterns of four thin films deposited from four individual targets at identical conditions – 15 W, Ar pressure of  $5 \times 10^{-3}$  mbar.

patterns of four GSST thin films deposited from the individual GSST targets under the same deposition conditions (15 W, Ar pressure of  $5 \times 10^{-3}$  mbar) fully confirms assumption described above.

### 3.2. Chemical composition

All the depositions together with indicated electrical power, Ar working pressure and composition determined by EDS are summarized in Table 1. EDS results indicate that some minor differences in composition may take part when the Ar working pressure increases from  $5 \times 10^{-3}$  mbar to  $1 \times 10^{-2}$  mbar. With respect to the target composition, it can be seen that the composition of the deposited films tends in general to be close to the nominal values of the target while experiencing an increase of Ge from 1% to 3%, relatively stable values ( $\sim +1\%$ – $2\%$ ) for antimony and tellurium, and a rather more significant decrease for selenium of about 3%–4%. Of course, these general trends will evolve more or less marginally with the variation of the composition and deposition parameters, which are for the latter relatively little adjustable in this work.

Looking in more detail at the composition change of the films, very similar trends can be noted for the first three films compositions with an average value of 21% for Ge and 18% Sb with related deviation of 1.1% and 0.6%, respectively and for which globally the Se deficit (of about  $-4\%$ ) and the small Te excess ( $+1\%$ – $2\%$ ) is respected from one film to another. A different behaviour is observed for the fourth, most Te-rich film, where a higher proportion of Sb (excess of  $+3\%$ ) compared to the target and lower concentration of Ge (19% on average, 1% deviation) compared with the other Se-richest films is consistently observed. This may be related to a somewhat enriched antimony concentration of the target itself for this (more difficult to fabricate) composition, but it would still appear that the increasing substitution of Te along the target compositions leads to a gradual increase in the proportion of antimony in the sputtered thin film.

The increase of Ar pressure slightly increases the amount of chalcogen elements, and thus the amount of heteropolar bonds in the films obtained when the Ar pressure increases from  $5 \times 10^{-3}$  to  $1 \times 10^{-2}$  mbar whatever the composition of the target and the applied power. An increased electrical power from 10 to 15 W at the same Ar pressure seems to increase the amount of heteropolar bonds to a smaller extent [24]. It has been shown in the literature for two Ge-Sb-Se targets with different ratio of Ge/Sb ( $R_{\text{Ge/Sb}} = 0.5$  and 4.5) that increasing the Ar pressure increases the content of selenium and decreases the germanium concentration, while the electrical power has a minor effect but can affect the antimony concentration in the case of a high Ge/Sb ratio [24,25]. For the GSST targets ( $R_{\text{Ge/Sb}} = 1.2$ ) with substitution of Se by Te, increasing Ar pressure or electrical power seems to increase the concentration of tellurium atoms (by 1% up to 2%) while the selenium content remains almost the same, perhaps slightly increased ( $+1\%$ ) but only with the effect of pressure and for the first three most selenium rich targets. The concentration of germanium and antimony has an expected behaviour considering the Ge/Sb ratio of these targets, [Sb] is indeed almost unaffected by Ar pressure and electric power while [Ge] tends to decrease slightly by 1–2% with Ar pressure and with electric power to a lesser extent. Therefore, for a given [Se/Te] ratio of the target, small compositional variation due to the change in pressure and electrical power could be responsible for minor changes in structure or optical properties.

### 3.3. Topography

AFM scans of  $1 \times 1 \mu\text{m}^2$  area of sputtered films having a thickness of 800 nm, represented by Fig. 2A–D, have shown that the root mean square (RMS) roughness ( $S_q$ ) of thin films surface increases with an

**Table 1**

Deposition parameters: sputtering targets nominal chemical composition (at. %), electrical power applied on the cathode (W) and Ar pressure in the deposition chamber ( $\times 10^{-3}$  mbar). Properties of the deposited thin films: deposition rate ( $\text{nm}\cdot\text{min}^{-1}$ ), chemical composition determined by EDS ( $\pm 1$  at. %), linear refractive index  $n_0$  at 1.55 and 7.7  $\mu\text{m}$  (both  $\pm 0.01$ ), and optical bandgap energy in eV determined by Cody-Lorentz oscillator model ( $E_g^{CL}$ ,  $\pm 0.02$  eV) from spectroscopic ellipsometry data analysis.

Theoretical target composition (at. %)	Power (W)	Ar pressure ( $\times 10^{-3}$ mbar)	Deposition rate ( $\text{nm}\cdot\text{min}^{-1}$ )	Thin film composition (at. %)	Linear refractive index $n_0$		$E_g^{CL}$ (eV)
					at 1.55 $\mu\text{m}$	at 7.70 $\mu\text{m}$	
<b>Ge<sub>19</sub>Sb<sub>17</sub>Se<sub>59</sub>Te<sub>5</sub></b>	10	5	9.9	Ge <sub>22</sub> Sb <sub>17</sub> Se <sub>55</sub> Te <sub>6</sub>	2.91	2.84	1.33
	10	10	10.4	Ge <sub>20</sub> Sb <sub>17</sub> Se <sub>56</sub> Te <sub>7</sub>	2.84	2.78	1.37
	15	5	19.8	Ge <sub>21</sub> Sb <sub>17</sub> Se <sub>55</sub> Te <sub>7</sub>	2.87	2.81	1.37
	15	10	20.0	Ge <sub>19</sub> Sb <sub>17</sub> Se <sub>56</sub> Te <sub>8</sub>	2.84	2.78	1.41
<b>Ge<sub>19</sub>Sb<sub>17</sub>Se<sub>54</sub>Te<sub>10</sub></b>	10	5	10.2	Ge <sub>22</sub> Sb <sub>18</sub> Se <sub>50</sub> Te <sub>10</sub>	2.97	2.89	1.27
	10	10	9.9	Ge <sub>20</sub> Sb <sub>17</sub> Se <sub>51</sub> Te <sub>12</sub>	2.91	2.83	1.33
	15	5	21.0	Ge <sub>21</sub> Sb <sub>18</sub> Se <sub>50</sub> Te <sub>11</sub>	2.96	2.88	1.25
	15	10	20.1	Ge <sub>20</sub> Sb <sub>18</sub> Se <sub>51</sub> Te <sub>11</sub>	2.91	2.84	1.27
<b>Ge<sub>19</sub>Sb<sub>17</sub>Se<sub>49</sub>Te<sub>15</sub></b>	10	5	10.0	Ge <sub>22</sub> Sb <sub>18</sub> Se <sub>45</sub> Te <sub>15</sub>	3.07	2.98	1.11
	10	10	10.1	Ge <sub>20</sub> Sb <sub>18</sub> Se <sub>46</sub> Te <sub>16</sub>	3.00	2.92	1.18
	15	5	20.4	Ge <sub>20</sub> Sb <sub>19</sub> Se <sub>45</sub> Te <sub>16</sub>	3.05	2.96	1.20
	15	10	20.7	Ge <sub>19</sub> Sb <sub>18</sub> Se <sub>46</sub> Te <sub>17</sub>	3.02	2.93	1.21
<b>Ge<sub>19</sub>Sb<sub>17</sub>Se<sub>44</sub>Te<sub>20</sub></b>	10	5	16.0	Ge <sub>20</sub> Sb <sub>20</sub> Se <sub>40</sub> Te <sub>20</sub>	3.20	3.09	1.05
	10	10	15.6	Ge <sub>18</sub> Sb <sub>20</sub> Se <sub>40</sub> Te <sub>22</sub>	3.17	3.06	1.12
	15	5	28.3	Ge <sub>19</sub> Sb <sub>20</sub> Se <sub>40</sub> Te <sub>21</sub>	3.18	3.07	1.05
	15	10	28.4	Ge <sub>18</sub> Sb <sub>20</sub> Se <sub>40</sub> Te <sub>22</sub>	3.14	3.04	1.08

increased tellurium content. Quantitatively, values of  $Sq$  increase from  $-0.3 \pm 0.1$  for Ge<sub>19</sub>Sb<sub>17</sub>Se<sub>59</sub>Te<sub>5</sub> (Fig. 2A) up to  $-0.9 \pm 0.1$  nm for Ge<sub>19</sub>Sb<sub>17</sub>Se<sub>44</sub>Te<sub>20</sub> (Fig. 2D). This is clearly caused by the presence of large grains for films with tellurium content above 15 at. %.

The work of Baudet et al. [25], studying the effect of decisive parameters of the sputtering process on the various properties of thin films in ternary Ge-Sb-Se system devoted to mid-IR sensor development, reports a significant variation of the roughness from

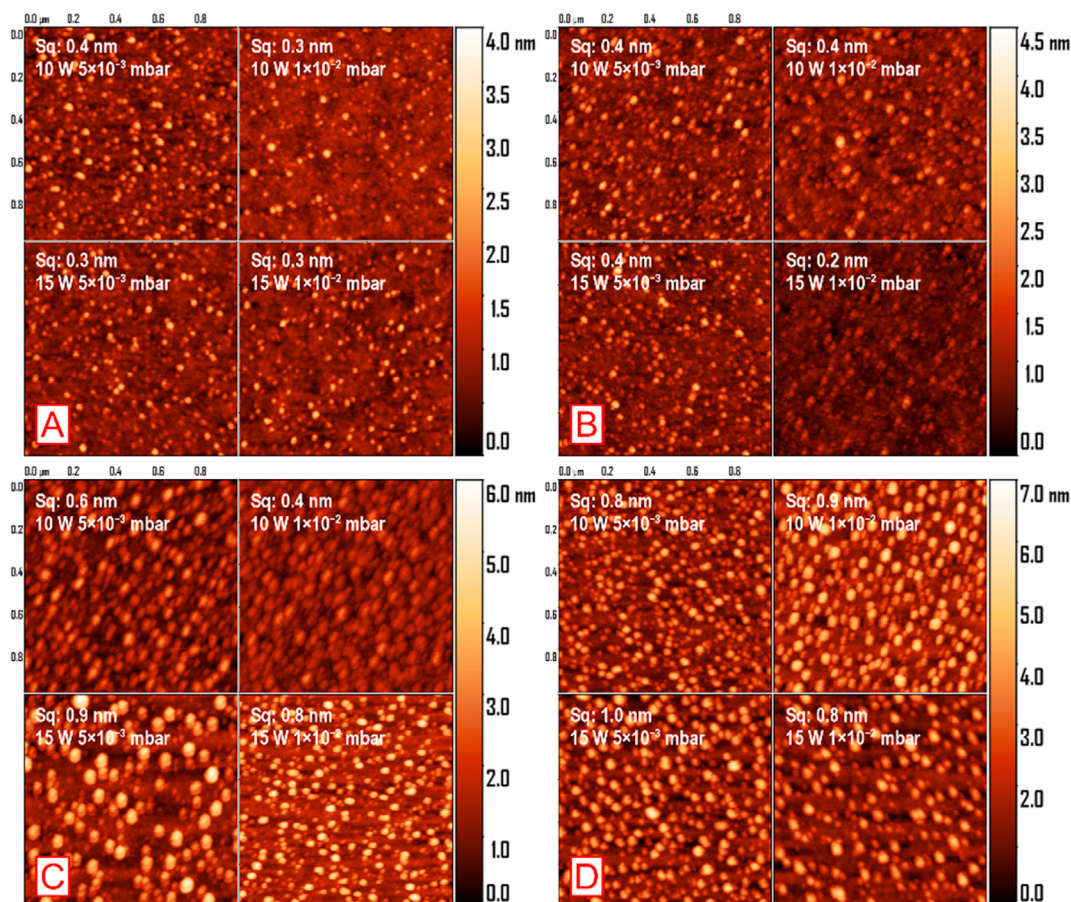


**Fig. 2.** AFM scans of  $1 \times 1 \mu\text{m}^2$  area of sputtered GSST thin films (with thickness of 800 nm) with indicated RMS roughness ( $Sq$ ,  $\pm 0.1$  nm), values on z-axis are normalized for each target nominal composition; A – Ge<sub>19</sub>Sb<sub>17</sub>Se<sub>59</sub>Te<sub>5</sub>, B – Ge<sub>19</sub>Sb<sub>17</sub>Se<sub>54</sub>Te<sub>10</sub>, C – Ge<sub>19</sub>Sb<sub>17</sub>Se<sub>49</sub>Te<sub>15</sub>, D – Ge<sub>19</sub>Sb<sub>17</sub>Se<sub>44</sub>Te<sub>20</sub>.

0.2 to 1 nm with a pressure varying from  $5 \times 10^{-3}$  to  $1 \times 10^{-2}$  mbar for the target composition richest in germanium considering an electric power lower than 17 W and a film thickness lower than 1  $\mu\text{m}$ . The composition richer in antimony is more stable in terms of roughness with Ar pressure variation. The addition of a few percent of tellurium to  $\text{Ge}_{19}\text{Sb}_{17}\text{Se}_{64}$  composition seems to make the roughness of the films relatively insensitive to the change of Ar pressure and to a lesser extent to the change of electrical power. To conclude, the roughness is essentially governed by the percentage of tellurium and could have a detrimental effect on the final optical losses of the photonics system used as a transducer for the IR medium optical sensor. It is therefore important, when selecting the ideal composition of the IR sensor's guiding layer, to make a compromise with the increasing introduction of tellurium between the gradual increase in roughness and the expected increase in both the increase in transmission in the IR domain and the refractive index in order to increase the index contrast and, consequently, the confinement of IR light.

### 3.4. Optical properties

**Linear refractive index and optical band-gap energy.** The effect of the [Te/Se] target ratio and deposition conditions on the optical properties, specifically linear refractive index ( $n_0$ ) and optical bandgap energy ( $E_g^{\text{CL}}$ ), were studied by spectroscopic ellipsometry. These results are summarized in Table 1. Moreover, the dispersion curves are shown in Fig. 3A–D. As seen, the substitution of selenium by heavier tellurium atoms, having higher polarizability, increases the linear refractive index. At the same time, the optical bandgap energy decreases as expected in accordance with semi-empirical Moss rule [26]. For the clarity, the dependencies of linear refractive index at 1.55 and 7.7  $\mu\text{m}$ , as well as the optical bandgap energy on the tellurium content are depicted in Fig. 4.

Values of refractive index at 7.7  $\mu\text{m}$  allow the evaluation of potential suitability of fabricated thin films for mid-infrared sensor application. Baudet et al. successfully applied chalcogenide thin films with composition  $\text{Ge}_{12.5}\text{Sb}_{25}\text{Se}_{62.5}$  as a waveguide guiding layer of the evanescent wave sensor for the detection of pollutants in water. The refractive index  $n_0$  at 7.7  $\mu\text{m}$  of these sputtered thin films is 2.77 ( $\pm 0.01$ ) and the refractive index contrast with the cladding layer is about 0.33 at 7.7  $\mu\text{m}$  for an Ar pressure of  $1 \times 10^{-1}$  mbar [25]. Among all used targets, the one with the composition  $\text{Ge}_{19}\text{Sb}_{17}\text{Se}_{59}\text{Te}_5$  seems to be suitable as a potential replacement of Te-free GSS target for the guiding layer. Thin film with composition  $\text{Ge}_{21}\text{Sb}_{17}\text{Se}_{55}\text{Te}_7$ , having values of  $n_0$  at 7.7  $\mu\text{m}$  and bandgap energy  $E_g^{\text{CL}}$  of 2.81 ( $\pm 0.01$ ) and 1.37 eV ( $\pm 0.02$ ), respectively, can potentially be used as a guiding layer for the evanescent wave sensors mentioned above [6]. Indeed, the refractive index contrast at 7.7  $\mu\text{m}$  between this thin film and a cladding layer with composition of  $\text{Ge}_{28.1}\text{Sb}_{6.3}\text{Se}_{65.6}$  used in such sensors would be 0.32 for the deposition parameters considered in this study (Table 1). Considering the deposition parameters, it can be noted that the linear refractive index decreases with an increasing argon pressure. Similar changes were observed by Baudet et al. in ternary Ge-Sb-Se thin films justified by changes in morphology and/or porosity as well as the roughness of sputtered films related to important variation of pressure between  $5 \times 10^{-3}$  to  $5 \times 10^{-2}$  mbar [25]. The effect of the latter was not proved in quaternary Ge-Sb-Se-Te as the AFM topography shows only small divergence when argon pressure was increased between  $5 \times 10^{-3}$  to  $1 \times 10^{-2}$  mbar only. The decrease of linear refractive index and the increase of  $E_g^{\text{CL}}$  with an increased pressure of argon in the variation range used for this study may be justified by other contributions and would be more related to the changes in composition of the GSST thin films.

As already mentioned, the increase in Ar pressure results in higher proportions of chalcogen atoms (Se and Te) compared to

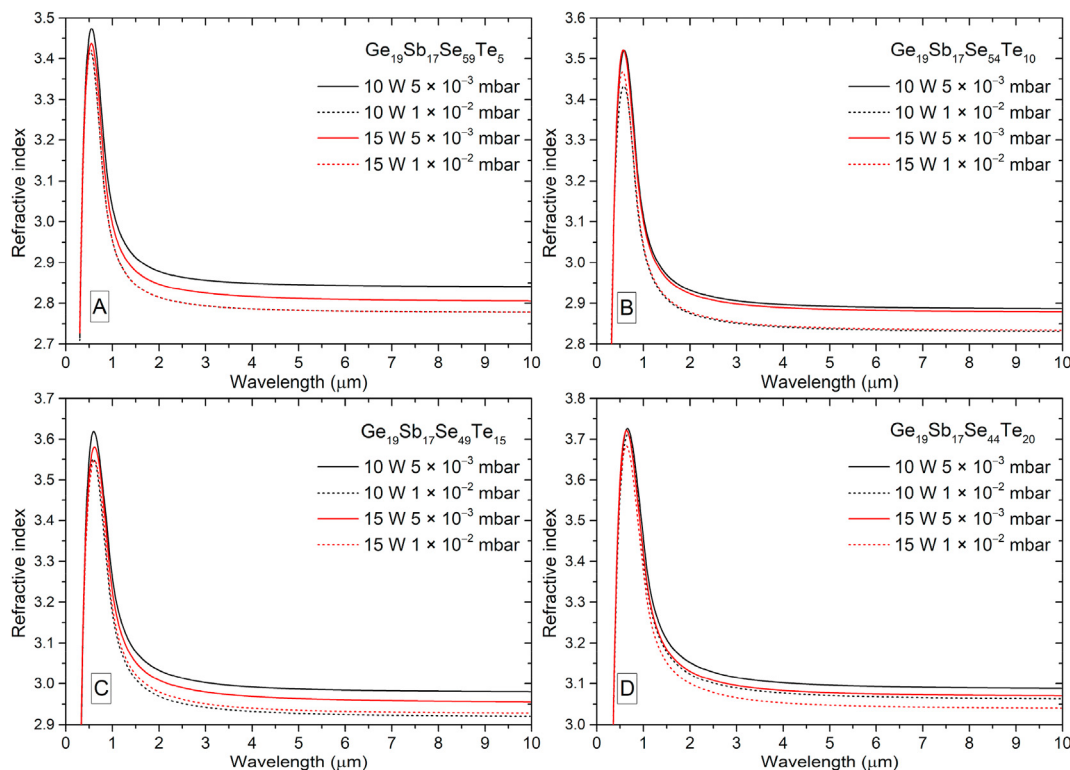
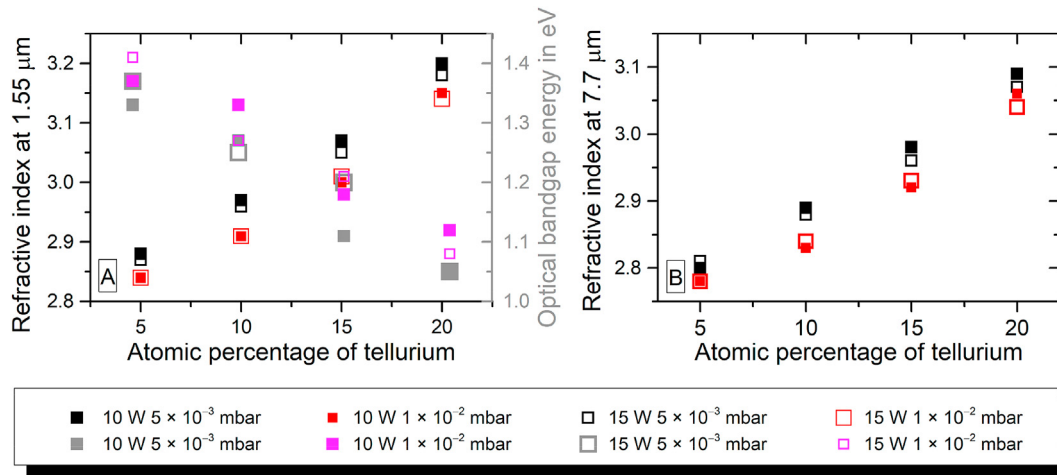


Fig. 3. Spectral dependencies of linear refractive indices of sputtered GSST thin films with indicated nominal compositions of the GSST target and deposition conditions.



**Fig. 4.** A – Dependence of linear refractive index at 1.55 μm and the optical bandgap energy  $E_g^{CL}$  on tellurium content, B – Dependence of linear refractive index at 7.7 μm on tellurium content.

metalloids (Ge, Sb) favouring the heteropolar bond formation. This leads to changes in  $n_0$  and  $E_g^{CL}$  as depicted in Fig. 4. The electrical power change from 10 to 15 W seems to have less significant effect on optical properties. The effect of the minor changes in compositions seems to have rather low effect on the fundamental absorption edge and thus reflects only small changes in the localized/tail states.

**NLO properties of GSST films.** The objective of nonlinear material selection for NLO devices should be a negligible linear absorption  $\alpha$ , the largest value of nonlinear refractive index ( $n_2$ ) and the smallest value of two photon absorption (TPA), defined by nonlinear absorption coefficient  $\beta$ , to optimize the nonlinear figure of merit ( $FOM = \frac{n_2}{\beta}$ ). According to classical modelling used to predict the nonlinear coefficients, like Sheik-Bahae method [27], the bandgap energy of amorphous chalcogenide thin films must be at least higher than  $\sim 1.6$  eV to obtain a negligible TPA at the 1.55 μm telecommunication wavelength. In selenide or seleno-telluride thin films, one can possibly consider for smaller  $E_g$  to be able to keep an interesting  $FOM$  if the  $n_2$  growth is faster than the TPA increase. The calculated values of nonlinear refractive index at telecommunication wavelength of 1.55 μm and at 7.7 μm mid-IR wavelength using Sheik-Bahae's formalism are plotted in Figs. 5A. Qualitatively, values of  $n_2$  at 1.55 μm decrease with increasing value of linear refractive index  $n_0$  while the opposite is true for  $n_2$  at 7.7 μm. This is due to the shape of the dispersion function for  $n_2$  within the used model, which becomes negative for approximately  $\hbar\omega \geq 0.7E_g$  when photon energy approaches resonance energy [28,29]. Consequently, the negative values of  $n_2$  at 1.55 μm were found for films  $Ge_{20}Sb_{20}Se_{40}Te_{20}$  ( $E_g^{CL} = 1.05$  eV,  $n_0 = 3.20$ ),  $Ge_{19}Sb_{20}Se_{40}Te_{21}$  ( $E_g^{CL} = 1.05$  eV,  $n_0 = 3.18$ ) and  $Ge_{18}Sb_{20}Se_{40}Te_{22}$  ( $E_g^{CL} = 1.08$  eV,  $n_0 = 3.14$ ). Similar observation was reported for some chalcogen poor and high Te concentration GSSTs by Dory et al. [28].

The maximum value of  $n_2$  at 1.55 μm, specifically  $28 \times 10^{-18} m^2 \cdot W^{-1}$ , was found for thin film with composition  $Ge_{20}Sb_{17}Se_{56}Te_7$  ( $E_g^{CL} = 1.37$  eV,  $n_0 = 2.84$ ,  $\beta = 2.2 \times 10^{-10} m \cdot W^{-1}$ ,  $FOM = 0.08$ ). Moreover, thin film with composition  $Ge_{19}Sb_{17}Se_{56}Te_8$  ( $E_g^{CL} = 1.41$  eV,  $n_0 = 2.84$ ,  $\beta = 1.6 \times 10^{-10} m \cdot W^{-1}$ ), having the same value of  $n_2$  shows the highest  $FOM$  at 1.55 μm among all fabricated GSST films (*i.e.* 0.11).

Overall, calculated values of nonlinear refractive index of deposited GSST films, ranging from 16 to  $28 m^2 \cdot W^{-1}$  (excluding negative values), are higher than reported calculated values of  $n_2$

for GSST thin films which are in the range from 5 to  $23 m^2 \cdot W^{-1}$  but the TPA coefficient ( $\beta$ ) is also expected to be higher [28]. Values of  $\beta$  at 1.55 μm for GSST are within the range of  $\sim 2-6 \times 10^{-10} m \cdot W^{-1}$  leading to  $FOM$  of  $\sim 0.01-0.11$  (excluding negative values due to negative  $n_2$ ). It should be noted that values of  $\beta$  in tellurium-free GSST having  $E_g^{CL} > 1.60$  eV are typically  $\sim 0.1 \times 10^{-10} m \cdot W^{-1}$  [30]. Nonlinear optical properties of GSST thin films studied in this work compared to available references are summarized in Table 2.

It should be mentioned that the calculated values of  $n_2$  and  $\beta$  in the present work are only order of magnitude estimations as the Sheik-Bahae's formalism is intended for the determination of Kerr coefficient and the two-photon absorption coefficient of direct-gap semiconductors. It should be kept in mind that amorphous chalcogenides are considered as non-direct gap materials and in this model, the tail and localized states related to amorphous materials are not taken into account, which is also the case for the Dinu model [34]. Moreover, the presence of uncertainties in the physical parameters used in the Sheik-Bahae's formalism enlarge the error in the estimation. It should be noted that calculated values of  $n_2$  obtained in this work are generally somewhat lower relative to those reported by Dory et al. [28]. In spite of this, used formalism allows to have a fairly good predictive vision on the  $n_2$  and  $\beta$  of amorphous chalcogenides by considering their refractive index and optical band-gap indicating trends that were verified experimentally for Ge-Sb-Se bulk glasses or thin films for which an error of experimental measurement of the order of  $\pm 10-20\%$  is expected [12,30,31,33]. For instance, Olivier et al. reported experimental values of nonlinear refractive index ( $n_2$ ) at 1.55 μm for bulk sample of  $Ge_{19.4}Sb_{16.7}Se_{63.9}$  glass around  $10 \pm 2.0 \times 10^{-18} m^2 \cdot W^{-1}$  and  $\beta$  around  $0.31 cm \cdot GW^{-1}$  obtained by direct transmission analysis [12]. Moreover, Kuriakose et al. reported experimental values (at 1.55 μm) of  $8 \pm 2 \times 10^{-18} m^2 \cdot W^{-1}$  ( $n_2$ ) and  $\beta$  around  $0.37 \pm 0.05 cm \cdot GW^{-1}$  for chalcogenide slab waveguides of 3 μm thickness prepared from  $Ge_{19.4}Sb_{16.7}Se_{63.9}$  target using beam self-trapping analysis [14]. Besides that, values of nonlinear refractive index calculated for GSST films are higher than those obtained for amorphous Ge-Sb-Se thin films with experimental values reaching the maximum value of  $n_2$  at 1.55 μm about  $21 \pm 3.0 \times 10^{-18} m^2 \cdot W^{-1}$  for amorphous  $Ge_3Sb_{35}Se_{62}$  [30]. The highest nonlinearity at 7.7 μm by means of  $n_2$  was found for thin film  $Ge_{19}Sb_{20}Se_{40}Te_{21}$  ( $E_g^{CL} = 1.05$  eV,  $n_0 = 3.18$ ). This is the consequence the strong TPA absorption at 1.55 μm in these films as depicted in Fig. 5B. To conclude, the trade-off between optical bandgap energy and the

**Table 2**

Comparison of nonlinear optical properties of GSST thin films with various references and with As<sub>2</sub>Se<sub>3</sub> bulk glass; chemical composition of thin films ( $\pm 1$  at. %), linear refractive index  $n_0$  at 1.55  $\mu\text{m}$  ( $\pm 0.01$ ), optical bandgap energy in eV ( $E_g^{\text{Cl}}$ ,  $\pm 0.02$  eV), nonlinear refractive index  $n_2$  ( $\times 10^{-18} \text{m}^2 \cdot \text{W}^{-1}$ ), TPA coefficient  $\beta$  ( $\times 10^{-10} \text{m} \cdot \text{W}^{-1}$ ) and FOM at 1.55  $\mu\text{m}$ .

Composition (at. %)	$n_0$ at 1.55 $\mu\text{m}$	$E_g^{\text{Cl}}$ (eV)	$n_2$ at 1.55 $\mu\text{m}$ ( $\times 10^{-18} \text{m}^2 \cdot \text{W}^{-1}$ )	$\beta$ at 1.55 $\mu\text{m}$ ( $\times 10^{-10} \text{m} \cdot \text{W}^{-1}$ )	FOM at 1.55 $\mu\text{m}$	Reference
Ge <sub>19</sub> Sb <sub>17</sub> Se <sub>56</sub> Te <sub>8</sub>	2.84	1.41	28	2	0.11	this work
Ge <sub>20</sub> Sb <sub>17</sub> Se <sub>51</sub> Te <sub>12</sub>	2.91	1.33	26	3	0.06	this work
Ge <sub>19</sub> Sb <sub>18</sub> Se <sub>46</sub> Te <sub>17</sub>	3.01	1.21	17	4	0.03	this work
Ge <sub>18</sub> Sb <sub>20</sub> Se <sub>40</sub> Te <sub>22</sub>	3.17	1.12	6	5	0.01	this work
Ge <sub>19</sub> Sb <sub>17</sub> Se <sub>64</sub>	2.68	1.86	8 $\pm$ 2	0.37 $\pm$ 0.05	0.14	[14]
Ge <sub>16</sub> Sb <sub>20</sub> Se <sub>64</sub>	2.69	1.68	9	N/A	0.56 <sup>a</sup>	[30]
Ge <sub>23</sub> Sb <sub>16</sub> Se <sub>61</sub>	2.67	1.65	11	N/A	0.73 <sup>a</sup>	[30]
Ge <sub>28</sub> Sb <sub>12</sub> Se <sub>60</sub>	2.66	1.66	11	N/A	0.70 <sup>a</sup>	[30]
Ge <sub>9</sub> Sb <sub>20</sub> Se <sub>71</sub>	2.76	1.68	10	N/A	0.65 <sup>a</sup>	[30]
Ge <sub>12</sub> Sb <sub>25</sub> Se <sub>63</sub>	2.80	1.65	11	N/A	0.73 <sup>a</sup>	[30]
Ge <sub>7</sub> Sb <sub>25</sub> Se <sub>68</sub>	2.86	1.61	13	N/A	0.86 <sup>a</sup>	[30]
Ge <sub>28</sub> Sb <sub>15</sub> Se <sub>52</sub> Te <sub>5</sub>	2.94	1.29	36	N/A	N/A	[28]
Ge <sub>40</sub> Se <sub>39</sub> Te <sub>21</sub>	2.92	1.26	44	N/A	N/A	[28]
Ge <sub>27</sub> Sb <sub>25</sub> Se <sub>48</sub>	2.79	1.34	25	N/A	N/A	[28]
As <sub>40</sub> Se <sub>60</sub>	2.80	1.70	9	N/A	0.58 <sup>a</sup>	[30]
As <sub>40</sub> Se <sub>60</sub> glass	2.78–2.84	1.74 <sup>b</sup>	12–13	0.25	~2	[31–33]

<sup>a</sup> Calculated according Sheik-Bahae with  $\beta = 0.1 \times 10^{-10} \text{m} \cdot \text{W}^{-1}$

<sup>b</sup> Tauc gap.

refractive index plays the crucial role when evaluating the nonlinear optical properties of materials. Lower optical bandgap energies of GSST relative to GSS thin films would indicate the possible limitation of these materials in terms of application in nonlinear optics at 1.55  $\mu\text{m}$  due to the high multi-photon absorption such as TPA absorption. This results in relatively low values of figure of merit 1.55  $\mu\text{m}$  as shown in Fig. 5B.

### 3.5. Wettability

Surface energy  $\sigma$  of thin films plays an important role when considering the potential application of these materials for chemical sensors. It is important to have an idea of the intrinsic surface energy before any functionalization of the chalcogenide film surface and the possible influence related to the tellurium concentration. Obtained contact angles for five standard liquids are summarized in Table 3. These were used for the calculation of values of dispersive  $\gamma_s^d$  and polar  $\gamma_s^p$  components together with the total surface energy  $\sigma$  of the GSST thin films using Owens-Wendt

theory (Fig. 6) –  $\gamma_s^d$  is obtained as a square of an intercept value and  $\gamma_s^p$  square of a slope value of a linear fit respectively.

As seen from Table 3, the values of surface energy for all the four compositions lie between  $\sim 37$  and  $39 \text{mJ} \cdot \text{m}^{-2}$ . These values are lower than those obtained by Baudet et al. for tellurium-free GSS thin films with the composition of Ge<sub>28.1</sub>Sb<sub>6.3</sub>Se<sub>65.6</sub> and Ge<sub>12.5</sub>Sb<sub>25</sub>Se<sub>62.5</sub> respectively. They obtained the values of about  $46 \text{mJ} \cdot \text{m}^{-2}$  for both compositions with negligible polar components ( $\sim 1 \text{mN} \cdot \text{m}^{-1}$ ) [10]. Moreover, Lucas et al. studied the contact angles of different liquids on polished bulk discs of Te<sub>20</sub>As<sub>30</sub>Se<sub>50</sub> glass for which the surface roughness is expected to be higher than chalcogenide thin films [35]. Quantitatively, they obtained the contact angles of  $73 \pm 3^\circ$  and  $62 \pm 3^\circ$  for water and glycerol respectively. The surface roughness rise usually increases the wettability as observed for these bulk chalcogenide glasses. In case of sputtered GSST films, the wettability just slightly increased when the tellurium content increases from 5 to 15 at. % for most of the used liquids. However, for the thin film with the tellurium content

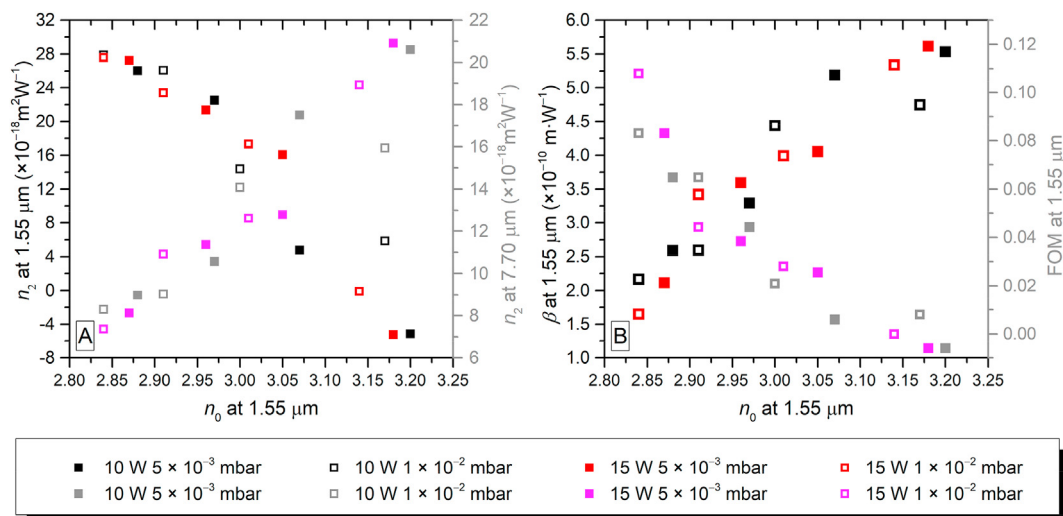


**Fig. 5.** (A) Dependence of nonlinear refractive index  $n_2$  on linear refractive index  $n_0$  at 1.55  $\mu\text{m}$ . (B) Dependence of TPA coefficient  $\beta$  and figure of merit  $FOM$  on linear refractive index  $n_0$  at 1.55  $\mu\text{m}$ .

**Table 3**

Compositions of GSST sputtered films determined by EDS ( $\pm 1$  at. %), RMS roughness ( $Sq$ ,  $\pm 0.1$  nm) obtained from AFM scans, contact angles for standard liquids, dispersive  $\gamma_s^d$  and polar  $\gamma_s^p$  components of surface energy obtained by Owens-Wendt theory (both  $\pm 2$  mN  $\cdot$  m $^{-1}$ ) and the values of surface energy  $\sigma$  ( $\pm 2$  mJ  $\cdot$  m $^{-2}$ ) of thin films.

Thin film composition (at. %)	$Sq$ (nm)	Contact angle, $\theta$ ( $^\circ$ )					$\gamma_s^d$ ( $\pm 2$ mN $\cdot$ m $^{-1}$ )	$\gamma_s^p$ ( $\pm 2$ mN $\cdot$ m $^{-1}$ )	$\sigma$ ( $\pm 2$ mJ $\cdot$ m $^{-2}$ )
		Water	ethylene glycol	formamide	glycerol	diiodomethane			
Ge <sub>22</sub> Sb <sub>17</sub> Se <sub>55</sub> Te <sub>6</sub>	0.4	70 $\pm$ 3	59 $\pm$ 1	61 $\pm$ 1	69 $\pm$ 1	41 $\pm$ 1	29	7	37
Ge <sub>22</sub> Sb <sub>18</sub> Se <sub>50</sub> Te <sub>10</sub>	0.4	71 $\pm$ 1	56 $\pm$ 1	61 $\pm$ 1	67 $\pm$ 1	42 $\pm$ 1	30	7	39
Ge <sub>22</sub> Sb <sub>18</sub> Se <sub>45</sub> Te <sub>15</sub>	0.6	68 $\pm$ 2	54 $\pm$ 2	61 $\pm$ 2	66 $\pm$ 2	39 $\pm$ 1	31	8	38
Ge <sub>20</sub> Sb <sub>20</sub> Se <sub>40</sub> Te <sub>20</sub>	0.8	54 $\pm$ 2	47 $\pm$ 1	51 $\pm$ 1	75 $\pm$ 1	54 $\pm$ 2	22	17	39

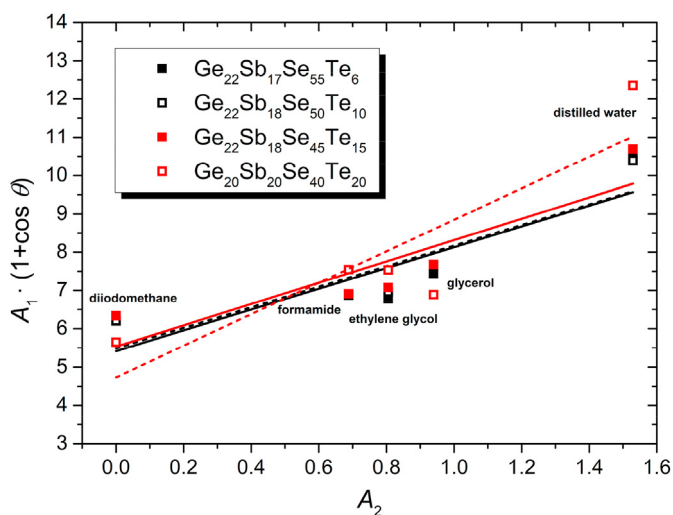


**Fig. 6.** Owens–Wendt plot for GSST thin films on silicon wafer with indicated nominal composition (10 W, 0.5 Pa);  $A_1 = \gamma_L/2\sqrt{\gamma_L^d}$  and  $A_2 = \sqrt{\gamma_L^p/\gamma_L^d}$ , where  $\gamma_L^d$  and  $\gamma_L^p$  stand for the dispersive and polar component of the surface tension of the standard liquid  $\gamma_L$ , respectively.

of 20 at. %. the contact angle is enlarged for glycerol and diiodomethane while for the others it is decreased. This causes the decrease of the intercept of the linear fit justified by the important decrease of the dispersive component of surface energy of this film as depicted in Fig. 6. In the same time, the small contact angle measured for the distilled water increases the slope of the linear fit enlarging the polar component of the surface energy of this film. The Ge<sub>19</sub>Sb<sub>17</sub>Se<sub>44</sub>Te<sub>20</sub> thin film seems to present an increased polarity of the surface, which might be explained by higher surface oxidation related to presence of tellurium in higher content or influence of surface roughness.

Surface oxidation can be a problem encountered for bulk glass, preform, optical fibers and thin films or waveguides based on chalcogenides. In order to prevent them from oxidation, many strategies are applied such as surface purification, distillation, chemical and mechanical polishing, cladding, coating, surface passivation, etc. Protection against the influence of the atmosphere by a chemical barrier layer can be performed during the manufacture of chalcogenide waveguides in order to limit optical losses, in particular by the deposition of Al<sub>2</sub>O<sub>3</sub>, Si<sub>3</sub>N<sub>4</sub> or SiO<sub>2</sub> on the surface if needed for photonics applications. However, it is first necessary to know well the chalcogenide material by taking care to characterize it before proceeding to the fabrication of the mentioned heterostructure to improve its performances. The nature of the specific surface of the thin films plays a preponderant role in this possible oxidation whatever the physical vapor deposition technique used [21,25,36].

In case of spectroscopic ellipsometry, the three-layer model is typically used consisting of substrate, film layer itself, and the

surface layer/roughness. The thicknesses of surface layer were fitted as  $\sim 1.6$ ,  $\sim 1.7$ ,  $\sim 1.6$  and  $\sim 2.2$  nm. Inherently, surface layer/roughness evaluated by ellipsometry is larger than surface roughness obtained from AFM. The thickness values of the surface layer/roughness shown above appear to be comparable to those of the sulphide/selenide thin films, which could lead to the conclusion that the seleno-telluride thin films do not oxidize more than the sulphides/selenides. Moreover, at such small thickness this oxide layer should not contribute significantly to optical losses. Nevertheless, further studies to discriminate between these two factors, i.e. surface oxidation and surface roughness, and to avoid any correlation effect should be conducted in future.

### 3.6. Local structure

The influence of the increasing tellurium content on the structure of thin films deposited at 10 W and Ar working pressure of  $5 \times 10^{-3}$  mbar is represented by the Raman scattering spectra shown in Fig. 7A. For a comparison, the spectra of sputtered thin film from Te-free Ge<sub>19</sub>Sb<sub>17</sub>Se<sub>64</sub> target deposited at 15 W at the same Ar working pressure is also shown.

For films sputtered from Ge<sub>19</sub>Sb<sub>17</sub>Se<sub>59</sub>Te<sub>5</sub> target, the Raman spectra are *prima facie* dominated by two contributions, the main peak at  $\sim 160$  cm $^{-1}$  with an adjacent asymmetric shoulder with the maxima at  $\sim 197$  cm $^{-1}$ . The two peaks shift gradually towards the lower wavenumbers with an increasing tellurium content in GSST thin films. As a result, the former is peaking at  $\sim 153$  cm $^{-1}$ , the latter at  $\sim 194$  cm $^{-1}$  in Ge<sub>19</sub>Sb<sub>17</sub>Se<sub>44</sub>Te<sub>20</sub>. The adjacent asymmetric shoulder (from 197 to 194 cm $^{-1}$ ) seems to find its origin in the symmetric stretching vibrations of Ge–Se bonds, typically at  $\sim 198$  and  $\sim 216$  cm $^{-1}$ , in corner-sharing and edge-sharing [GeSe<sub>4</sub>] tetrahedra, respectively.

In the Raman spectra of Te-free Ge<sub>19</sub>Sb<sub>17</sub>Se<sub>64</sub> thin film, this peak ( $\sim 200$  cm $^{-1}$ ) and its shoulder ( $\sim 214$  cm $^{-1}$ ) are better observed. For this pure selenide film, they are mainly accompanied by an additional shoulder (at  $\sim 175$  cm $^{-1}$ ) related to Ge–Ge stretching modes in [GeSe<sub>4-y</sub>Ge<sub>y</sub>] distorted tetrahedra with  $y = 1, 2, 3$  and ethane-like Se<sub>3</sub>Ge–GeSe<sub>3</sub>. They are also complemented by an important contribution (at  $\sim 190$  cm $^{-1}$ ) of Sb–Se stretching mode of [SbSe<sub>3</sub>] pyramids and probably vibration modes related to Ge–Sb bonds around 165 cm $^{-1}$  [12,24] and finally by a small broad band observed between 250 and 315 cm $^{-1}$  with several contributions mainly from (Se–Se) stretching mode from  $\sim 245$  cm $^{-1}$ – $\sim 265$  cm $^{-1}$  coming from  $-(\text{Se–Se})_n-$  long chains to  $-(\text{Se–Se})-$  dimers and also  $\nu_{\text{as}}$  [GeSe<sub>4</sub>] [37] (Fig. 7-A).

In the case of the GSST thin films, these different bands and shoulders related to [GeSe<sub>4</sub>], Ge–Ge and Se–Se vibration modes seem to disappear gradually with the [Te] increase to the profit of the main band at lower frequency. In the structure of multicomponent glasses and thin films which contain more than one chalcogen element, mixed entities such as [GeSe<sub>4-x</sub>Te<sub>x</sub>] and [SbSe<sub>3-x</sub>Te<sub>x</sub>] can be at the origin of the main broad peak observed at  $\sim 160$  cm $^{-1}$  as referred by Abdellaoui et al. in quinary



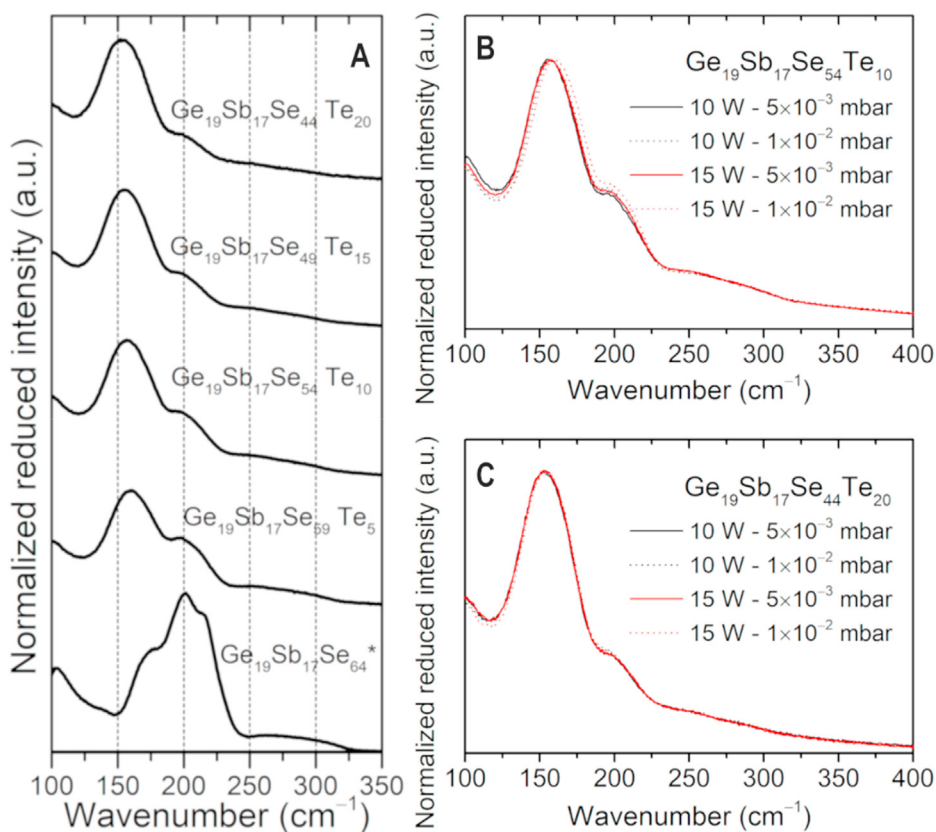


**Fig. 7.** Raman spectra of sputtered GSST thin films: A – indicated theoretical target compositions (\* from Ref. [13]), and deposition conditions: B – Target  $\text{Ge}_{19}\text{Sb}_{17}\text{Se}_{54}\text{Te}_{10}$ , C – Target  $\text{Ge}_{19}\text{Sb}_{17}\text{Se}_{44}\text{Te}_{20}$ .

$\text{Ga}_5\text{Ge}_{20}\text{Sb}_{10}\text{Se}_{65-x}\text{Te}_x$  ( $x = 10\text{--}37.5$  at. %) bulk glasses [38] and by Gonçalves et al. for ternary  $\text{Ge}_{20}\text{Te}_{80-x}\text{Se}_x$  bulk glass [37]. The broad band can have also non negligible contributions related to the presence of Ge(Sb)–Ge(Sb) bonds because the GSST films present a deficit in selenium as observed for Te-free  $\text{Ge}_{19}\text{Sb}_{17}\text{Se}_{64}$  with vibrational modes localized from 150 (mainly related to vibration modes of (Sb–Sb) bond in  $\text{SbSe}_2\text{--SbSe}_2$  entities) to  $175\text{ cm}^{-1}$  [12,24,39].

Even if the GSST films present a deficit of selenium, the presence of Se–Te and even Te–Te can be envisaged, as Se–Se bonds are present in small proportion in  $\text{Ge}_{19}\text{Sb}_{17}\text{Se}_{64}$  thin film. It can be noted that vibration modes of (Te–Te) bond from  $-(\text{Te–Te})_n$  chains to dimer possess vibrational modes in the range from 145 to  $165\text{ cm}^{-1}$  [40] and might slightly contribute to the main broad bands centered at  $160\text{ cm}^{-1}$  while vibrational modes of (Te–Se) bonds inside mixed chains or mixed dimers could present vibration modes in the range of  $208\text{--}266\text{ cm}^{-1}$  [37,41]. It was proposed in the case of  $\text{Ge}_{20}\text{Te}_{80-x}\text{Se}_x$  chalcogen rich glass that the substitution of Te to Se in small proportion will lead to the introduction of Te inside the  $-(\text{Se–Se})_n-$  chains before to bond  $[\text{GeSe}_4]$  tetrahedra forming finally mixed entities when the tellurium increases. It could be also the case in the GSST films but it is important to keep in mind that the chemical composition of the  $\text{Ge}_{19}\text{Sb}_{17}\text{Se}_{64-x}\text{Te}_x$  targets is stoichiometric and the GSST films present a deficit of selenium compare to the targets. Apart from bonding defects generated by a statistical disorder inherent to amorphous chalcogenides, the selenium deficit limits the chalcogen–chalcogen bonds occurrence while it substantially should increase the proportion of Ge(Sb)–Ge(Sb) bonds. All mixed entities and homopolar bond modifications will have an important impact on the electronic band

structure and localized/tail states of amorphous GSST thin films and on the hyperpolarizability of the entities and bonds present in the amorphous lattice substantially modifying their bandgap  $E_g$  and nonlinear properties.

Moreover, the Raman spectra of GSST films are strongly affected when tellurium is introduced even in small proportion, as it was also observed in stoichiometric  $\text{Ga}_5\text{Ge}_{20}\text{Sb}_{10}\text{Se}_{65-x}\text{Te}_x$  glasses much more rapidly than in the case of a system rich in chalcogen [37,41]. Thus, the shift of the main broad band from  $160\text{ cm}^{-1}$  to  $153\text{ cm}^{-1}$  can be mainly explained by the increase of the substitution of Se by Te in the mixed entities as  $[\text{GeTe}_4]$  present a stretching vibration mode centered at  $130\text{ cm}^{-1}$  [37,40,42] and  $[\text{SbTe}_3]$  pyramidal units or defective octahedral present Raman active band at  $145\text{ cm}^{-1}$  [43].

The changes of deposition conditions by means of the increased electrical power and/or argon pressure do not seem to affect the local structure significantly and less and less with tellurium content increase. The pressure and electrical power increase have an effect on  $\nu_s[\text{GeSe}_4]$  intensity with a slight increase and on the position of the main band at  $160\text{ cm}^{-1}$  slightly shifted to higher wavenumber.

#### 4. Conclusions

GSST thin films were fabricated by rf magnetron sputtering from glass or glass-ceramics targets with nominal composition of  $\text{Ge}_{19.4}\text{Sb}_{16.7}\text{Se}_{63.9-x}\text{Te}_x$  ( $x = 5, 10, 15, 20$ ). The structure of GSST amorphous films according to Raman analysis seems to be built mainly by selenide and mixed entities in variable proportion according to the tellurium concentration such as  $[\text{GeSe}_{4-x}\text{Te}_x]$  and  $[\text{SbSe}_{3-x}\text{Te}_x]$  ( $x = 0, 1, 2$ ) and in all likelihood homopolar Ge(Sb)–

Ge(Sb) bonds to compensate for the chalcogen deficiency. The contact angle measurements have shown values of 68–71° for water of the GSST thin films resulting in values of surface energy of about ~36–39 mJ · m<sup>-2</sup>. The presence of 20 at. % of tellurium increases the polar component of the surface energy of the thin film and decrease the contact angle to 54° which might be related to the oxidation of the surface in link with the composition and also roughness increase. Analysis of ellipsometric data revealed the increase of linear refractive index with increasing tellurium concentration while the optical bandgap energy decreases. Moreover, the former seems to decrease with the increasing working pressure of argon from 5 × 10<sup>-3</sup> to 1 × 10<sup>-2</sup> mbar, which is mainly related to the composition changes. The electrical power change from 10 to 15 W seem to have insignificant effect. Among all used targets, the one with the composition Ge<sub>19</sub>Sb<sub>17</sub>Se<sub>59</sub>Te<sub>5</sub> seems to be suitable as a potential replacement of Te-free GSS target for the guiding layer. Indeed, the refractive index contrast at 7.7 μm between a GSST thin film and a cladding layer with composition of Ge<sub>28.1</sub>Sb<sub>6.3</sub>Se<sub>65.6</sub> used in such sensors would be at least equal to 0.32. By adjusting the Te/Se composition, it is possible to control the index contrast between the guiding layer and the buffer layer in order to create an efficient IR sensor in terms of evanescent fields and with compact dimensions.

Furthermore, it was shown that thin film with composition Ge<sub>19</sub>Sb<sub>17</sub>Se<sub>56</sub>Te<sub>8</sub>, having nonlinear refractive index  $n_2 \sim 28 \times 10^{-18} \text{ m}^2 \cdot \text{W}^{-1}$ , shows the highest FOM at 1.55 μm among all fabricated films. Calculated values of  $n_2$  for GSST films are within the range from 16 to 28 × 10<sup>-18</sup> m<sup>2</sup> · W<sup>-1</sup> (excluding negative values). The potential limitation of these materials when the concentration in tellurium increase may lie in low values of optical bandgap energies resulting in high two-photon absorption at telecommunication wavelength (*i.e.* 1.55 μm) which will not be the case for mid-IR. To conclude, wide IR transparency in combination with high (non)linear refractive indices make these materials suitable for potential applications in the field of mid-infrared devices such as optical switches and sensors.

## Funding

This work was supported by the CNRS, Brittany region (France), ANR LOUISE (ANR-15-CE04-0001-01), ANR AQUAE (ANR-21-CE04-0011) and Czech Science Foundation (Project No. 19-24516S).

## Declaration of competing interest

The authors declare that they have no known competing financial interests or personal relationships that could have appeared to influence the work reported in this paper.

## Acknowledgements

Platform Spectroscopy Infrared and Raman (SIR – ScanMAT, Université de Rennes 1) and CMEBA are acknowledged for performed Raman and EDS measurements, respectively.

## References

- [1] Ovshinsky SR, Klose PH. Amorphous and Liquid Semiconductors Imaging in amorphous materials by structural alteration. *J Non-Cryst Solids* 1972;8: 892–8.
- [2] Savage JA, Nielsen S. Chalcogenide glasses transmitting in the infrared between 1 and 20 μ — a state of the art review. *Infrared Phys* 1965;5(4): 195–204.
- [3] Tanaka K. Optical nonlinearity in photonic glasses. In: Kasap S, Capper P, editors. *Springer handbook of electronic and photonic materials*. Cham: Springer International Publishing; 2017. 1–1.
- [4] Wuttig M, Yamada N. Phase-change materials for rewriteable data storage. *Nat Mater* 2007;6(11):824–32.
- [5] Tang J, Yuan F, Shen X, Wang Z, Rao M, He Y, Sun Y, Li X, Zhang W, Li Y, Gao B, Qian H, Bi G, Song S, Yang JJ, Wu H. Bridging biological and artificial neural networks with emerging neuromorphic devices: fundamentals, progress, and challenges. *Adv Mater* 2019;31(49):1902761.
- [6] Baudet E, Gutierrez-Arroyo A, Baillieul M, Charrier J, Nèmec P, Bodiou L, Lemaitre J, Rinnert E, Michel K, Bureau B, Adam JL, Nazabal V. Development of an evanescent optical integrated sensor in the mid-infrared for detection of pollution in groundwater or seawater. *Adv Device Mater* 2017;3(2):23–9.
- [7] Nguyen HPT, Tuan TH, Xing L, Matsumoto M, Sakai G, Suzuki T, Ohishi Y. Supercontinuum generation in a chalcogenide all-solid hybrid micro-structured optical fiber. *Opt Express* 2020;28(12):17539–55.
- [8] Sharma N, Sharda S, Sharma V, Sharma P. Far-infrared investigation of ternary Ge–Se–Sb and quaternary Ge–Se–Sb–Te chalcogenide glasses. *J Non-Cryst Solids* 2013;375:114–8.
- [9] Ganjoo A, Jain H, Khalid S, Pantano CG. Structural modification of Ge–Se amorphous films with the addition of Sb. *Phil Mag Lett* 2005;85(10):503–12.
- [10] Baudet E, Gutierrez-Arroyo A, Nèmec P, Bodiou L, Lemaitre J, De Sagazan O, Lhermitte H, Rinnert E, Michel K, Bureau B, Charrier J, Nazabal V. Selenium sputtered films development for MIR environmental sensor. *Opt Mater Express* 2016;6(8):2616–27.
- [11] Delcourt E, Jebali N, Bodiou L, Baillieul M, Baudet E, Lemaitre J, Nazabal V, Dumeige Y, Charrier J. Self-phase modulation and four-wave mixing in a chalcogenide ridge waveguide. *Opt Mater Express* 2020;10(6):1440–50.
- [12] Olivier M, Tchahame JC, Nèmec P, Chauvet M, Besse V, Cassagne C, Boudebs G, Renversez G, Boidin R, Baudet E, Nazabal V. Structure, nonlinear properties, and photosensitivity of (GeSe<sub>2</sub>)<sub>100-x</sub>(Sb<sub>2</sub>Se<sub>3</sub>)<sub>x</sub> glasses. *Opt Mater Express* 2014;4(3):525–40.
- [13] Baillieul M. Infrared sensors for aquatic pollutants : synthesis, optimization and qualification, vol. 1. Université de Rennes; 2018.
- [14] Kuriakose T. Demonstration of the spatial self-trapping of a plasmonic wave. *Bourgogne Franche-Comté*; 2018.
- [15] Sharma N, Sharda S, Katyal SC, Sharma V, Sharma P. Effect of Te on linear and non-linear optical properties of new quaternary Ge-Se-Sb-Te chalcogenide glasses. *Electron. Mater. Lett.* 2014;10(1):101–6.
- [16] Singh PK, Lohia P, Dwivedi DK. Investigation of dielectric relaxation and a.c. conductivity of third generation multi-component Ge<sub>10-x</sub>Se<sub>60</sub>Te<sub>30</sub>Sb<sub>x</sub> (0 ≤ x ≤ 6) chalcogenide glasses. *J Mater Sci Mater Electron* 2019;30(14): 13797–809.
- [17] Wang H, Guo T, Xue Y, Lv S, Yao D, Zhou Z, Song S, Song Z. The phase change memory features high-temperature characteristic based on Ge-Sb-Se-Te alloys. *Mater Lett* 2019;254:182–5.
- [18] Zhang Y, Chou JB, Li J, Li H, Du Q, Yadav A, Zhou S, Shalaginov MY, Fang Z, Zhong H, Roberts C, Robinson P, Bohlin B, Rios C, Lin H, Kang M, Gu T, Warner J, Liberman V, Richardson K, Hu J. Broadband transparent optical phase change materials for high-performance nonvolatile photonics. *Nat Commun* 2019;10(1):4279.
- [19] Wang G, Nie Q, Wang X, Shen X, Chen F, Xu T, Dai S, Zhang X. New far-infrared transmitting Te-based chalcogenide glasses. *J Appl Phys* 2011;110(4):043536.
- [20] Zhang S, Zhang X-h, Barillot M, Calvez L, Boussard C, Bureau B, Lucas J, Kirschner V, Parent G. Purification of Te<sub>75</sub>Ga<sub>10</sub>Ge<sub>15</sub> glass for far infrared transmitting optics for space application. *Opt Mater* 2010;32(9):1055–9.
- [21] Charpentier F, Dussauze M, Cathelinaud M, Delaizir G, Kamitsos EI, Adam JL, Bureau B, Nazabal V. Aging process of photosensitive chalcogenide films deposited by electron beam deposition. *J Alloys Compd* 2011;509(27): 7330–6.
- [22] Shuker R, Gammon RW. Raman-scattering selection-rule breaking and the density of states in amorphous materials. *Phys Rev Lett* 1970;25(4):222–5.
- [23] Ferlauto AS, Ferreira GM, Pearce JM, Wronski CR, Collins RW, Deng X, Ganguly G. Analytical model for the optical functions of amorphous semiconductors from the near-infrared to ultraviolet: applications in thin film photovoltaics. *J Appl Phys* 2002;92(5):2424–36.
- [24] Baudet E, Cardinaud C, Girard A, Rinnert E, Michel K, Bureau B, Nazabal V. Structural analysis of RF sputtered Ge-Sb-Se thin films by Raman and X-ray photoelectron spectroscopies. *J Non-Cryst Solids* 2016;444:64–72.
- [25] Baudet E, Sergent M, Nèmec P, Cardinaud C, Rinnert E, Michel K, Jouany L, Bureau B, Nazabal V. Experimental design approach for deposition optimization of RF sputtered chalcogenide thin films devoted to environmental optical sensors. *Sci Rep* 2017;7(1):3500.
- [26] Moss TS. A relationship between the refractive index and the infra-red threshold of sensitivity for photoconductors. *Proc Phys Soc Lond B* 1950;63(363):167–76.
- [27] Sheik-Bahae M, Van Stryland EW. *Semiconductors and semimetals*. San Diego: E. Garmire, A. Kost; 1999 [Chapter 4].
- [28] Dory JB, Castro-Chavarria C, Verdy A, Jager JB, Bernard M, Sabbione C, Tessaire M, Fédéli JM, Coillet A, Cluzel B, Noé P. Ge–Sb–S–Se–Te amorphous chalcogenide thin films towards on-chip nonlinear photonic devices. *Sci Rep* 2020;10(1):11894.
- [29] Tanaka K. Nonlinear optics in glasses: how can we analyze? *J Phys Chem Solid* 2007;68(5):896–900.
- [30] Halenkovič T, Gutwirth J, Kuriakose T, Bouška M, Chauvet M, Renversez G, Nèmec P, Nazabal V. Linear and nonlinear optical properties of co-sputtered Ge-Sb-Se amorphous thin films. *Opt Lett* 2020;45(6):1523–6.
- [31] Lenz G, Zimmermann J, Katsufuji T, Lines ME, Hwang HY, Spalter S, Slusher RE, Cheong SW, Sanghera JS, Aggarwal IDon. Large Kerr effect in bulk Se-based

- chalcogenide glasses. *Opt Lett* 2000;25(4):254–6.
- [32] Ta'eed VG, Baker NJ, Fu L, Finsterbusch K, Lamont MRE, Moss DJ, Nguyen HC, Eggleton BJ, Choi DY, Madden S, Luther-Davies B. Ultrafast all-optical chalcogenide glass photonic circuits. *Opt Express* 2007;15(15):9205–21.
- [33] Wang T, Gai X, Wei W, Wang R, Yang Z, Shen X, Madden S, Luther-Davies B. Systematic z-scan measurements of the third order nonlinearity of chalcogenide glasses. *Opt Mater Express* 2014;4(5):1011–22.
- [34] Dinu M. Dispersion of phonon-assisted nonresonant third-order nonlinearities. *IEEE J Quant Electron* 2003;39(11):1498–503.
- [35] Lucas P, Solis MA, Coq DL, Juncker C, Riley MR, Collier J, Boesewetter DE, Boussard-Plédel C, Bureau B. Infrared biosensors using hydrophobic chalcogenide fibers sensitized with live cells. *Sensor Actuator B Chem* 2006;119(2):355–62.
- [36] Verger F, Nazabal V, Colas F, Némec P, Cardinaud C, Baudet E, Chahal R, Rinnert E, Boukerma K, Peron I, Deputier S, Guilloux-Viry M, Guin JP, Lhermite H, Moreac A, Compère C, Bureau B. RF sputtered amorphous chalcogenide thin films for surface enhanced infrared absorption spectroscopy. *Opt Mater Express* 2013;3(12):2112–31.
- [37] Gonçalves C, Mereau R, Nazabal V, Boussard-Plédel C, Roiland C, Furet E, Deschamps M, Bureau B, Dussauze M. Study of the Ge<sub>20</sub>Te<sub>80</sub>-xSex glassy structures by combining solid state NMR, vibrational spectroscopies and DFT modelling. *J Solid State Chem* 2021;297:122062.
- [38] Abdellaoui N, Starecki F, Boussard-Plédel C, Shpotyuk Y, Doualan JL, Braud A, Baudet E, Némec P, Chevirié F, Dussauze M, Bureau B, Camy P, Nazabal V. Tb<sup>3+</sup>-doped Ga<sub>5</sub>Ge<sub>20</sub>Sb<sub>10</sub>Se<sub>65</sub>-xTex (x = 0–37.5) chalcogenide glasses and fibers for MWIR and LWIR emissions. *Opt Mater Express* 2018;8(9):2887–900.
- [39] Petit L, Carlie N, Richardson K, Guo Y, Schulte A, Campbell B, Ferreira B, Martin S. Effect of the substitution of S for Se on the structure of the glasses in the system Ge<sub>0.23</sub>Sb<sub>0.07</sub>Se<sub>0.70</sub>-xSex. *J Phys Chem Solid* 2005;66(10):1788–94.
- [40] Sen S, Gjersing EL, Aitken BG. Physical properties of GexAs<sub>2</sub>xTe<sub>100–3x</sub> glasses and Raman spectroscopic analysis of their short-range structure. *J Non-Cryst Solids* 2010;356(41):2083–8.
- [41] Mendoza-Galvan A, Garcia-Garcia E, Vorobiev YV, Gonzalez-Hernandez J. Structural, optical and electrical characterization of amorphous SeTe thin film alloys. *Microelectron Eng* 2000;51–52:677–87.
- [42] Voleská I, Akola J, Jóvári P, Gutwirth J, Wágner T, Vasileiadis T, Yannopoulos SN, Jones RO. Structure, electronic, and vibrational properties of

glassy Ga<sub>11</sub>Ge<sub>11</sub>Te<sub>78</sub>: experimentally constrained density functional study. *Phys Rev B* 2012;86(9):094108.

- [43] Sosso GC, Caravati S, Mazzarello R, Bernasconi M. Raman spectra of cubic and amorphous Ge<sub>2</sub>Sb<sub>2</sub>Te<sub>5</sub> from first principles. *Phys Rev B* 2011;83(13):134201.



Tomáš Halenkovič: currently working as an assistant professor at the Department of Graphic Arts and Photophysics, Faculty of Chemical Technology at the University of Pardubice, Czech Republic. He obtained his Ph.D. under joint supervision between the University of Pardubice, Czech Republic and University of Rennes 1, France. He is a laureate of Czech Ministry of Education, Youth and Sports Award 2019 in the category of Ph.D. students and Ph.D. graduates. He was also a visiting researcher at University of Mons in Belgium in 2021. Main focus of his research is aimed on optical properties and photoinduced phenomena in amorphous chalcogenide thin films.



Virginie Nazabal is a research director at CNRS (France). She received her Ph.D. in solid state chemistry from the University of Bordeaux in 1999, after a master's degree and a bachelor's degree from the Ecole Normale Supérieure, University of Paris VI (now Paris-Sorbonne University). She joined NIMS (Tsukuba, Japan) for her post-doctoral training in 2000 and 2001 concerning combinatorial chemistry in glass science. Her research activity at CNRS is devoted to glasses and amorphous materials for photonics at the Institute of Chemical Sciences of the University of Rennes. She received a bronze medal from CNRS in 2010. She is involved in various research projects at national and international level and is co-author of more than 200 publications. During the last 10 years, she has

developed activities concerning glass materials in the field of infrared optical sensors (Pollutec-Ademe Prize 2011, Innovative techniques for the environment), mid-infrared fluorescent sources and nonlinear photonics.